Photoelectron spectra of $Gd_2O_2^-$ and non-monotonic photon-energy dependent variations in populations of close-lying neutral states

Jarrett L. Mason[†], Hassan Harb[‡], Ali Abou Taka[‡], Abbey J. McMahon[†], Caleb D. Huizenga[†], Hector Corzo[‡], Hrant P. Hratchian*[‡], and Caroline Chick Jarrold*[†]

[†]*Department of Chemistry, Indiana University, 800 E. Kirkwood Ave, Bloomington, IN, 47405*
[‡]*Department of Chemistry and Chemical Biology, University of California, Merced, 5200 North Lake Road, Merced, CA 95343*
FOR SUBMISSION TO NATURE CHEMISTRY

ABSTRACT

Photoelectron spectra of $Gd_2O_2^-$ obtained with photon energies from 2.033 eV to 3.495 eV exhibit numerous close-lying neutral states with photon-energy-dependent relative intensities. Transitions to states falling within the electron binding energy window of 0.9 and 1.6 eV are attributed to one- or two-electron transitions to the ground and low-lying excited neutral states. An additional, manifold of electronic states observed in the 2.1 to 2.8 eV window cannot be assigned to any simple one-electron transitions. Because of the relatively simple electronic structure from the half-filled $4f^7$ subshell occupancy in $Gd_2O_2^-$, the numerous transitions observed in the spectra are fairly well-resolved, allowing a detailed view of the changes in relative intensities of individual transitions with photon energy. With supporting calculations on the numerous close-lying electronic states, we suggest a description of strong photoelectron-valence electron interactions that result in the photon-energy dependent shake-up transitions and switching between ferro- and antiferromagnetic coupling.

---

* email: Hrant P. Hratchian hhratchian@ucmerced.edu; Caroline Chick Jarrold cjarrold@indiana.edu

INTRODUCTION

Electron correlation is central to the electronic structures and properties of matter, and enhancing our understanding of strongly correlated electronic materials is a prominent theme of scientific grand challenges. The lanthanides (*Ln*) have proven to be fertile ground in this arena,[1] with *Ln* atomic ions, molecules, and materials finding applications in the areas of quantum simulators[2] and single molecule magnets,[3] the latter of which is associated with potential application in spintronics materials.[4] The *Ln* $4f^n$ series is characterized by elements having similar chemical properties, for as the atomic number increases, the occupancy of the contracted and nuclear-shielding $4f^n$ subshell increases.

Partially-filled $4f^n$ subshells and close-lying 5d and 6s orbitals give rise to a rich constellation of close-lying, nearly identical electronic states. If we consider *Ln*O diatomic molecules, in which the valence orbital occupancy can be described in general terms as $[\sigma_{2p}^2\ \pi_{2p}^4]\ 4f^n\ \sigma_{6s}$, numerous close-lying states associated with the coupling between the 4f and σ_{6s} electrons, and the manifold states associated with the projection of j_f and j_{6s} onto the internuclear axis (Ω). As an example, CeO ($4f^1\ \sigma_{6s}$) has 16 states within a 0.5 eV window of energy,[5-7] SmO ($4f^5\sigma_{6s}$) has 30 states in the same window, plus tens more slightly higher in energy.[8] EuO ($4f^7$) and GdO ($4f^7\ \sigma_{6s}$), near the center of the row are much simpler, having one and two states arising from those occupancies, respectively, because of the zero-orbital angular momentum associated with the half-filled 4f (^8S) subshell.[8]

Electron correlation is also an important governing factor in photoionization and photodetachment processes. We recently reported unusual phenomena observed in the anion photoelectron (PE) spectra of Sm_xO_y suboxide ($y \leq x$) cluster anions, along with mixed Ce-Sm suboxides. Specifically, we observed a striking increase in the relative intensities of excited states with decreasing photon energy (decreasing electron kinetic energy, e^-KE),[9-11] opposite of the Wigner threshold law.[12] This effect was most pronounced in clusters with average oxidation states of the metal centers in the clusters being less than or

equal to +2, and it was not at all observed in pure cerium oxide clusters of any stoichiometry. This result suggested that the higher density of states associated with the Sm center contributed to the effect.

Resonance with excited anion states embedded in the detachment continuum can have pronounced effects on the intensities of detachment transitions, with a few examples included in the references.[13-18] However, the underlying source of the changes in excited state intensities in the case of these samarium-containing suboxide clusters appeared to be shake-up transitions or internal inelastic scattering from strong photoelectron-valence electron (PEVE) interactions. To explore this effect in more detail, we demonstrated an increase in the relative intensity of an unresolved manifold of excited state transitions in the Sm_2O^- PE spectrum that was inversely proportional to the momentum of the photoelectrons by measuring the spectrum over a range of photon energies.[19] The trend of increasing excited state intensity with decreasing momentum additionally showed a broad oscillation that was likely due to a shape resonance. Overall, however, the effect was largely interpreted as PEVE interactions, which we attributed to the very high density of electronic states in a narrow window for Sm_2O, associated with the $4f^5$ or $4f^6$ subshell occupancy, the latter being predicted to be the lower lying configuration in DFT calculations.

In this report, we present a new and striking example of this intriguing inverse-threshold phenomenon by examining the $Gd_2O_2^-$ cluster. We hypothesized this system would provide a useful canvas for exploring the fundamental physics of this effect due to the much simpler electronic structure afforded by the $4f^7$ subshell occupancy. Based on DFT calculations, $Gd_2O_2^-$ is expected to have D_{2h} symmetry, with the two O-atoms bridging the Gd centers which are separated by *ca*. 3.1 Å. As depicted in Figure 1, the highest occupied orbitals are the in- and out-of-phase combination of the Gd 6s orbitals (a_g and b_{1u}, symmetries, respectively). According to the calculations, the spin projection is entirely along the Gd–Gd axis. Therefore, for simplicity, we will forego the D_{2h} symmetry terms, and refer to the non-bonding Gd-local orbitals arising from 6s and 5d orbitals by their symmetry with respect to the Gd–Gd axis ($\sigma_{6s,g}$, $\sigma_{6s,u}$, $\delta_{5d,g}$ etc.).

As shown schematically in Figure 1, the $\sigma_{6s,g}$, $\sigma_{6s,u}$, can be described as outer-valence orbitals. Covalent bonds are formed from the O 2p and Gd 5d orbitals, and are predicted to be more than 3 eV lower in energy, while the core-like non-bonding Gd 4f orbitals are an additional 2 eV lower in energy. Analogous to the GdO diatomic, the general electronic structure of the neutral can be described as two Gd^{2+} centers with $4f^7 6s^1$ electronic configurations. In an isolated Gd^{2+} atom, the half-filled 4f subshell would be a spherically symmetric, high spin core. Some polarization away from the O centers is expected in the Gd_2O_2 anion and neutral, but the overall contribution of the 4f orbitals to the electronic term would be a_g. The anion has an additional electron in the outer-valance 6s-based orbital, and a $^{16}B_{1u}$ electronic term would result from ferromagnetically (FM) coupled 4f ^{7} centers; a $^2B_{1u}$ term would arise from

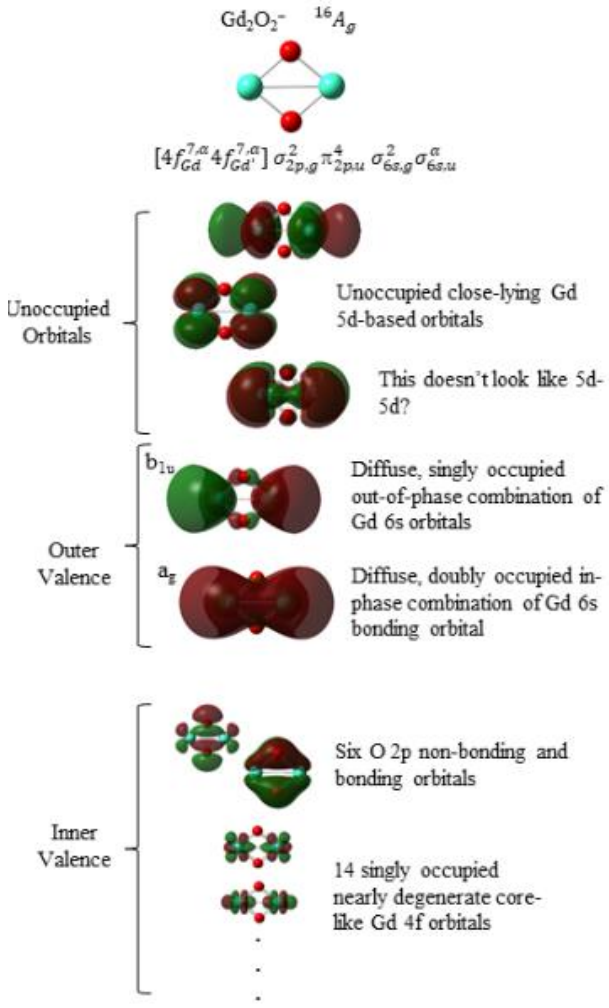

Figure 1. Molecular and electronic structure of the lowest energy state of $Gd_2O_2^-$ computed using the B3LYPANO-ECPplusPVTZ method.

antiferromagnetically (AFM) coupled centers and is calculated to be 0.07 eV higher in energy. The paramagnetism in di-Gd complexes has made them effective MRI contrast agents.[20]

Given this electronic structure, the detachment spectrum is expected to exhibit three close-lying one-electron transitions associated with detachment of any of the three outer valence electrons. Because the orbitals are diffuse and non-bonding, the anion and neutral should have nearly identical structures, yielding vertical detachment transitions. Additional nearly-vertical transitions would be observed if the ion beam were also populated with the AFM-coupled $^{2}B_{1u}$ state or the lower-spin $^{14}B_{1u}$ state arising from antiparallel alignment between the outer-valence electron and the (FM-coupled) $4f^{7}$ electrons.

In contrast, the PE spectra of $Gd_2O_2^-$ collected with photon energies ranging from 2.033 eV to 3.495 eV do not exhibit three simple, near-vertical transitions. Rather, they exhibit two distinct manifolds of close-lying electronic transitions, and the emergence of two-electron transitions with decreasing e^-KE. Unlike the results for Sm_2O^-, the relative excited state intensities do not change smoothly with photon energy. We consider the effect of the ejected electrons' electric field on the highly polarizable outer valence orbitals as well as the relative stability of the FM and AFM states, along with larger zero-field splitting parameter in particular spin states of neutral Gd_2O_2.

RESULTS

Figure 2 shows the PE spectra of $Gd_2O_2^-$ collected using (a) 3.495 eV, (b) 3.024 eV, (c) 2.621 eV, and (d) 2.033 eV photon energies. In all four panels, the darker colored traces are spectra collected with laser polarization parallel to the electron drift path, and the lighter colored traces with perpendicular polarization. The spectra are plotted as a function of electron binding energy, $e^-BE = h\nu - e^-KE$, which, unlike the electron kinetic energy, e^-KE, is independent of photon energy and allows for direct comparison of transitions to a given neutral state. Pale vertical lines running between the four panels connect common transitions observed at all four detachment energies.

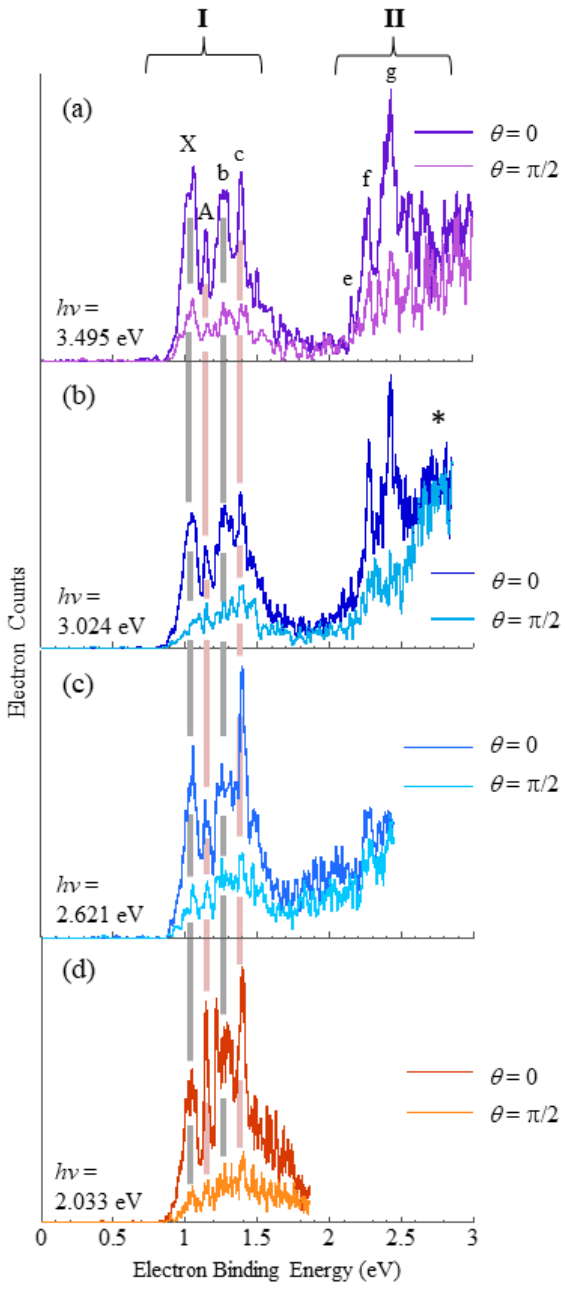

Figure 2. Anion PE spectra of $Gd_2O_2^-$ measured using (a) 3.495 eV, (b) 3.024 eV, (c) 2.621 eV, and (d) 2.033 eV photon energies. Darker colors are spectra measured with laser polarization parallel to the electron drift path, lighter colors with perpendicular polarization. Peak positions for manifolds **I** and **II** are included in Table 2. Vertical rose and gray lines are included to guide the eye between transitions common to all four spectra.

The spectra all show a group of transitions between 0.9 eV and 1.6 eV (manifold **I**), with fairly parallel photoelectron angular distributions (PADs). Additional transitions are observed above 2 eV (manifold **II**)

in spectra obtained with higher photon energies. All spectra are included in the supplementary information.

A general trend in the spectra measured with different photon energies is an increase in the relative intensities of higher e^-BE (excited state) transitions with decreasing photon energies, in apparent violation of the Wigner threshold law; we note that this behavior resembles previous results on Sm_2O^-.[19] However, in contrast to the Sm_2O^- spectra, many of the numerous electronic transitions are well-resolved, allowing the observation of non-monotonic change in relative intensity with photon energy.

Transitions in manifold I in the 3.495 eV PE spectrum: Based on previous work,[21-29] homo- and heteronuclear lanthanide oxide cluster anions with average metal oxidation state less than +3 exhibit photodetachment transitions around $e^-BE \approx 1$ eV. The transitions can be described as creating a hole in a 6s-based molecular orbital. They are characterized by large photodetachment cross sections and parallel PADs. Manifold **I** in the $Gd_2O_2^-$ spectrum shares these characteristics.

The spectrum measured with the highest photon energy, 3.495 eV, is most appropriately interpreted in the "sudden" detachment framework.[19,30] We therefore make an initial assignment of manifold **I** on the basis of the appearance of this spectrum [Figure 2(a)]. Additional features in the $Gd_2O_2^-$ spectrum emerge in manifold **I** in the spectra measured with lower photon energies, as described below.

There are four distinct features in manifold **I** in Figure 2(a), labeled X, A, b, and c. X and b are broader than A and c, and the X-b and A-c energy splitting is very similar to the $X\,^9\Sigma^- - a\,^7\Sigma^-$ splitting in the GdO diatomic (0.23 eV).[31,32] The states of the diatomic both have $4f^7\,\sigma_{6s}$ electronic configurations and differ only in the spin of the electron in the σ_{6s} orbital. It is therefore tempting to assign these two sets of peaks to transitions associated with detaching either an α or β electron from one of the σ_{6s} MOs of Gd_2O_2. However, this splitting *also* coincides with the energy interval between two narrow and intense features observed in the much simpler PE spectrum of $Ce_2O_2^-$; in neutral Ce_2O_2, the coupling between the

electrons occupying the 6s-based orbitals and the electrons singly occupying a 4f orbital on the two separate Ce centers is *ca.* 0.01 eV, and the 0.23 eV observed splitting was attributed to the difference in energy associated with detaching the electron from the $\sigma_{6s,g}$ and $\sigma_{6s,u}$ orbitals. The four features therefore suggests a combination of splitting between possible spin states and the splitting between different states accessed by detachment from the $\sigma_{6s,g}$ and $\sigma_{6s,u}$ outer valence orbitals.

As a starting point, we consider the computational results summarized in Figure 3 and Table 1 (a comprehensive listing of the anion and neutral states is included in the supplementary information). Table 1 also includes calculations on the GdO^- and GdO diatomics, along with previously reported experimental and ligand field theory results.[8] The reasonable agreement between DFT, LFT and experiment provides a measure of validation for the DFT calculations in predicting the energy ordering of the states. As shown in Figure 3, the highest spin anion $^{16}B_{1u}$ is predicted to be the lowest energy state, with the AFM-coupled analog, $^{2}B_{1u}$, state lying 0.07 eV higher. The small energy difference calls into question the identity of the true ground state. However, calculations including spin projection models predict the $^{2}B_{1u}$ state to be 0.09 eV higher than the $^{16}B_{1u}$ state, and calculations with varying degrees of exact exchange (B3LYP, BLYP, B3PW91, and M062x) all gave similar results, with AFM excitation energies ranging from 0.06 to 0.08 eV. The $^{14}B_{1u}$ state, in which the spin of the electron in the $\sigma_{6s,u}$ orbital is antiparallel to the 4f electrons, is predicted to be 0.18 eV higher in energy than the $^{16}B_{1u}$ ground state, which is reasonable considering the 0.23 eV $^{7}\Sigma - {}^{9}\Sigma$ splitting in GdO.

Neutral states are situated above the anion states that connect to them by strictly one-electron detachment transitions in Figure 3. A noteworthy result is that the lowest energy electronic state of the neutral is the $^{1}A_g$ (AFM-coupled) state, which is predicted to be 0.78 eV above the $^{16}B_{1u}$ state; the one-electron $^{1}A_g \leftarrow {}^{2}B_{1u}$ transition would be observed at $e^-BE \approx 0.7$ eV. This result, however, calls into question how accurately DFT calculations quantitatively predict the difference in energy for the $^{1}A_g$ and $^{15}A_g$ states (0.78 eV versus 1.08 eV). Coupling between the $4f^7$ cores in dincuclear Gd(III) complexes is small, with

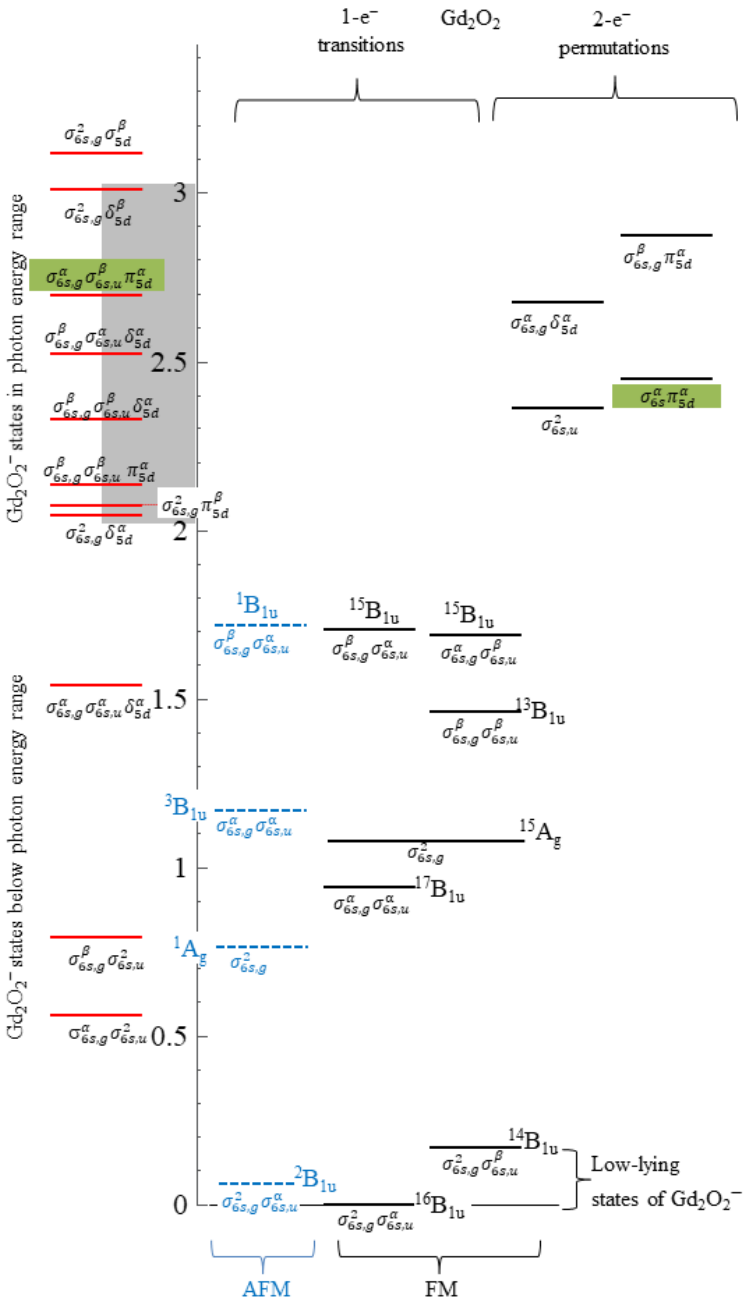

Figure 3. Schematic of the relative energies of the low-lying AFM- (blue dashed lines) and FM-coupled (black solid lines) anion and neutral states of Gd_2O_2, along with several higher-energy excited states of $Gd_2O_2^-$, including several lying within the experimental photon energy range (gray box). The states indicated by green boxes are connected by one-electron loss of the anion.

energy differences between the FM- and AFM-coupled states on the order of 1 cm^{-1},[33] though additional electrons in the outervalence orbitals may increase the coupling .[34,35] In the case of the ^1A_g and $^{15}A_g$ states, the outervalence electrons are paired. In contrast, the $^{17}B_{1u}$ state is predicted to be lower in energy than its

AFM $^{3}B_{1u}$ analog, and similarly, the FM-coupled $^{16}B_{1u}$ state is predicted to be lower in energy than its AFM $^{2}B_{1u}$ analog, which suggests that unpaired outer-valence electrons stabilize FM coupling between the $4f^{7}$ cores.

Both the $^{16}B_{1u}$ ground state and $^{14}B_{1u}$ excited state have three one-electron accessible neutral states predicted in a ~0.9 to 1.7 eV window of energy above the $^{16}B_{1u}$ state, the $^{15}A_{g}$ state being a common final state, for a total of five neutral FM-coupled states. Representative Natural Ionization Orbitals (NIOs) are included in the supplementary information, and support the picture of detachment transitions involving only the outer valence electrons. The open-shell 15-tets are predicted to be nearly isoenergetic at 1.70 eV. We note that the AFM-coupled analog to the open shell 15-tet states, the $^{1}B_{1u}$ state, is also calculated to be very close in energy to these three $^{15}B_{1u}$ states.

A simulation invoking a rigid one-electron detachment assumption and identical detachment cross sections for every transition is shown in Figure 4(a). The intensities of transitions from the $^{14}B_{1u}$ state are Boltzmann weighted assuming an excitation energy of 0.18 eV and a liberal temperature of 1000K. We also assume the AFM-coupled $^{2}B_{1u}$ state is not present in the ion beam. The spectrum is dominated by three transitions from the $^{16}B_{1u}$ state. Three predominant transitions do not qualitatively agree with the spectrum. The cryo-SEVI spectrum of SmO^{-} reported by Weichman et al.[36] exhibited a number of transitions that fall outside of the rigid one-electron picture. If we include transitions to all five FM-coupled states, which implies that the four $^{2S+1}B_{1u}$ states are mixed and that spin is not a good quantum number, the simulation [Figure 4(b)] does have four pronounced transitions, one of which involves overlapping transitions to the two nearly isoenergetic open-shell $^{15}B_{1u}$ states. Electronic hot bands shown also assume the $^{14}B_{1u}$ state can access all five neutral F-coupled states.

Agreement between the simulations and the transitions in manifold **I** is not perfect. The energy range in which the simulated transitions are predicted to lie is ca. 0.3 eV broader than the observed transitions,

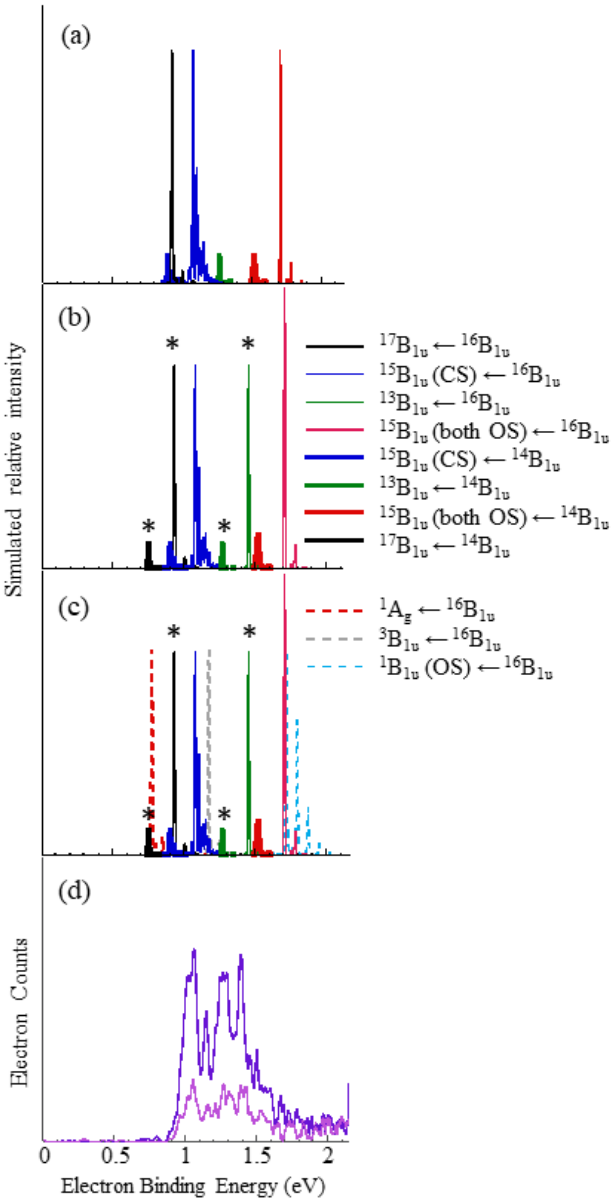

Figure 4. (a) Spectral simulations of the three strictly one-electron transitions accessible from the $^{16}B_{1u}$ state of $Gd_2O_2^-$ along with temperature-weighted one-electron transitions accessible from the $^{14}B_{1u}$ state. (b) Transitions to all low-lying neutral states originating from the $^{16}B_{1u}$ and (temperature weighted) $^{14}B_{1u}$ states assuming relaxation of $\Delta s = \pm ½$ spin selection rule (c) Added to the simulations in (b), transitions to the AFM-coupled spin states. (d) PE spectrum obtained using 3.495 eV included for comparison.

though this magnitude of error is typical for detachment transition energies.[37] In addition, the individual detachment transitions are predicted to be nearly vertical, as expected from the diffuse, non-bonding

character of the $\sigma_{6s,g}$ and $\sigma_{6s,u}$ orbitals, whereas bands X and b are broadened. Interestingly, based on the calculated relative energies of the neutral states, bands X and b would be assigned to the $^{17}B_{1u}$ and $^{13}B_{1u}$ states, both of which have parallel alignment of the electron spins in the outer-valence $\sigma_{6s,g}$ and $\sigma_{6s,u}$ orbitals (all other states predicted in this energy range have antiparallel spins). Zero-field splitting in the $^{9}\Sigma^{+}$ state of the GdO ($4f^{7}\ \sigma_{6s}$) state is sub-cm^{-1},[38] and tri-nuclear Gd complexes have coupling between the $4f^{7}$ centers on the order of 0.2 cm^{-1},[39] which is comparable to a simple classical calculation of the energy difference between $M_s = 15$ and $M_s = 0$ FM coupled Gd $4f^{7}$ subshells in the calculated Gd_2O_2 structure presented here (~1 cm^{-1}). However, additional coupling from the unpaired electrons in the outer-valence orbitals may come into play. Indeed, magnetic exchange coupling constants determined for digadolinium complex anions have been reported to be as high as –27 cm^{-1}.[34,35] If we assume that a range of M_s values are accessed in the photodetachment transition (*vide infra*), a value of D = –15 cm^{-1} would account for the breadth of bands X and b. The simulated transitions to these states that may be broadened by large zero-field splitting are indicated with asterisks (*). Note, however, that band X could also be fit with a harmonic frequency of 217 cm^{-1} and an anharmonicity of 3 cm^{-1}, though again, the predicted vertical appearance of the transitions is consistent with the chemical intuition on detachment from non-bonding orbitals.

Manifold II is not assignable to one-electron transitions: Manifold **II** is somewhat puzzling, since transitions involving detachment from the inner valence orbitals are expected to be several eV higher in energy, whereas manifold **II** is approximately 1.2 eV higher in energy. The relative intensities of the transitions in manifold **II** are different from manifold **I**, but the peak spacings within the two manifolds are similar. The intensities of transitions in manifold **II** increase relative to manifold **I** with decreasing photon energy from 3.495 eV to 2.924 eV, as can be seen in the contour plot in Figure 5, which shows the relative intensities of all the spectra (collected with $\theta = 0^{o}$ laser polarization) after normalizing all the spectra over manifold **I**. Such anti-threshold law behavior was a hallmark of strong electron-neutral interactions observed in previous studies.[10,11,19]

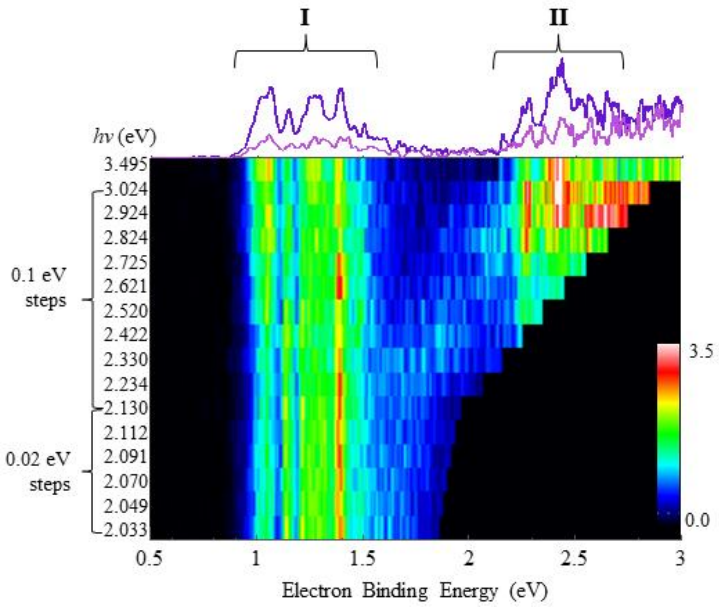

Figure 5. Contour plot showing the intensities of transitions in spectra measured with different photon energies. All spectra were normalized between the energies of 0.8 eV and 1.8 eV. The spectrum measured using 3.495 eV is shown across the top of the plot to guide the eye.

The position of manifold **II** relative to manifold **I** is nearly identical to a group of excited state transitions observed in the PE spectrum of GdO^-, which had been assigned to final neutral states with $4f^7$ 6p occupancies.[32] Our own calculations on GdO excited states (Table 1) suggest that the final state has $4f^7$ $5d_\delta$ occupancy, but either way, the transitions are better described as shake-up transitions, where electron promotion accompanies electron detachment. We note here that lower-intensity signal at similar e^-BE values in numerous $Ln_xO_y^-$ (*Ln* = Ce, Pr, Sm, Eu) suboxide clusters has been observed, and attributed to shake-up transitions.[9-11,21,23-25]

Included in Figure 3 are the relative energies of excited states that differ by more than one electron from the $^{16}B_{1u}$ anion (beyond spin of the electrons in the outer valence orbitals). For example, considering the $\sigma_{6s,g}^2\sigma_{6s,u}^\alpha$ occupancy of the $^{16}B_{1u}$ anion ground state, the $\sigma_{6s,u}^2$ $^{15}A_g$ neutral state would be accessed by detaching an electron from the $\sigma_{6s,g}$ orbital while promoting the remaining $\sigma_{6s,g}$ electron to the $\sigma_{6s,u}$ orbital. The calculations predict this transition to be at 2.35 eV, which falls within the energy range of

manifold **II**. Similarly, detachment accompanied by promotion of an electron into the non-bonding combinations of the Gd 5d orbitals would fall in a similar energy range.

Why are shake-up transitions prevalent and commonly observed in the spectra of lanthanide oxides with multiply occupied 6s-based orbitals?[9,10,21,23-25] We consider the possibility of strong PEVE interactions. The diffuse 6s-based outer-valence orbitals are highly polarizable. Drawing from previous work,[10,11,19] we hypothesize that the electric field from the ejected electron transiently polarizes these orbitals, which would then be described as a time-dependent superposition of outer-valence orbitals. Using the example of the $\sigma_{6s,u}^2$ $^{15}A_g$ final neutral state above, detachment of a $\sigma_{6s,g}$electron from the $\sigma_{6s,g}^2\sigma_{6s,u}^{\alpha}$ $^{16}B_{1u}$ would nominally yield the $^{17}B_{1u}$ in the sudden approximation, but while the electron is proximal to the neutral, the perturbed $\sigma'_{6s,g}$ orbital could be described as

$$\sigma'_{6s,g}(t) = c_1(t)\sigma_{6s,g} + c_2(t)\sigma_{6s,u} + \cdots + c_i(t)\varphi_i$$

If, for example, the electron is ejected along the Gd-Gd axis, $c_2(t)$ would be transiently large, and the probability of populating the final state in which an electron populates the $\sigma_{6s,u}$ would follow. A similar rationale was posited by Wang and coworkers in their elegant description of polarization of valence orbitals by a dipole-bound electron.[40] A distinction between a dipole bound electron and an ejected electron is the time-dependent nature of the latter; decreasing the photon energy and, hence, the photoelectron momentum, increases the time over which the orbital mixing occurs.

While we calculated four neutral states in the energy range of manifold **II**, the close-lying 6p and 5d orbitals on the two Gd centers will give rise to many additional states. Therefore, we will not attempt to make specific assignments, and will instead generally point to two-electron transitions. We note that there are also numerous excited anion states in the range of photon energies spanned in this study, shown schematically by red lines in Figure 3, raising the possibility of resonance enhancements. For example, the state described by the $\sigma_{6s,g}^{\alpha}\sigma_{6s,u}^{\beta}\pi_{5d}^{\alpha}$ occupancy (shaded green) could be accessed by a dipole-allowed

transition from the $^{16}B_{1u}$ state (assuming spin is not a good quantum number) followed by loss of the $\sigma^{\beta}_{6s,u}$ electron, which would be more akin to a conjugate shake-up transition (dipole-driven electron excitation, monopole detachment), which becomes more prevalent near threshold.[41,42]

Emergence of additional photon-energy dependent transitions in manifold I. The vertical axis on the contour plot in Figure 5 is not evenly incremented, as labeled. However, it is evident that features within manifold **I** are also changing significantly both over 0.1 eV steps (2.130 eV ≤ *hν* ≤ 3.024 eV) and 0.02 eV steps (2.033 eV ≤ *hν* ≤ 2.130 eV). An expanded view of manifold **I** is shown in Figure 6, along with several spectra obtained using different photon energies and parallel polarization. Several distinct features are labeled, and the positions of the transitions are summarized in Table 2.

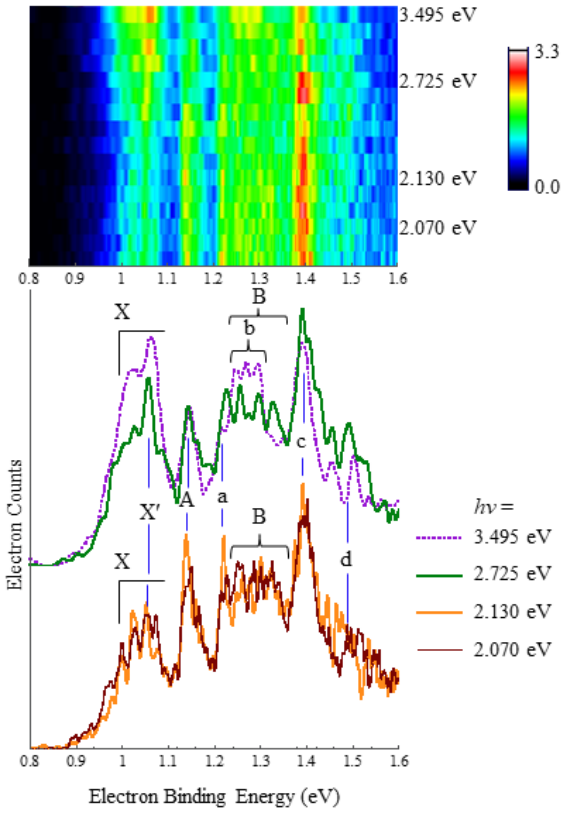

Figure 6. Contour plot of PE spectra measured with different photon energies plotted on an expanded scale to highlight manifold **I**, along with representative spectra measured at four different energies to illustrate changes in relative intensities over wider energy steps (purple and green) and a smaller, 0.06 eV step (orange and maroon). Positions of features labeled on the spectra are summarized in Table 2.

As noted previously, the lowest binding energy feature, X, is relatively broad, and at lower photon energies exhibits partially resolved, ~220 cm^{-1} spacings on the low e^-BE rising edge that converge with increasing e^-BE, suggesting significant anharmonicity or splitting between M_s levels of the $^{17}B_{1u}$ neutral state. The profile of this band is affected by X′, a narrow feature at 1.05 eV that is pronounced in several, but not all, spectra collected using photon energies between 2.422 through 2.924 eV. Bands X and b in the 3.495 eV spectrum in Figure 5 [indicated by the gray vertical lines, Figure 2] are separated by 1840 cm^{-1} and have similar profiles, as noted above. However, with lower photon energies, band b is engulfed in a broader collection of close-lying features, labeled B, which itself changes profile with photon energy. Bands A and c [indicated by the rose vertical lines, Figure 2] are narrower and both increase in intensity relative to band X with decreasing photon energy, apparently uncorrelated. Transition a, appearing as a lower intensity shoulder in the 3.495 eV spectrum, grows in intensity with decreasing photon energy and appears to be correlated with variations in the intensity of band A.

The intensity changes with photon energy are not monotonic, and are in some cases anti-correlated, which suggests that either excited state resonances or interference between different shake-up channels are occurring. Again, as seen in Figure 3, there are a number of excited anion states that fall within the photon energy range used in this study, and many of these states (all FM-coupled) could undergo resonant electronic excitation followed by autodetachment of the excited electron, enhancing the final neutral state intensity formed from autodetachment. However, the total number of transitions that appear to be varying in intensity with photon energy exceeds the five FM-states calculated to lie in this energy range.

Given the sharp features in manifold **I** grow in intensity (though not monotonically) with decreasing photon energy, we consider the possibility that slower photoelectrons interact with the remnant neutral Gd_2O_2 in a way that switches FM-states to AFM-states. The relative stability of FM and AFM states can switch in the presence of an external electric field,[43–48] raising the possibility that the electric field from the photoelectron temporarily affects the neutral state energies. Treating the detachment process as

sudden implies that the electron is instantaneously at much greater distances, leaving the magnetic moment unaffected. However, at the lowest photon energies, the electron would require several fs to escape the range of the outer-valence orbitals, generating an electric field radially pointing toward an electron of 3.6 $V \cdot Å^{-1}$ at a 2 Å distance, which is considerable. The electric field could temporarily stabilize the AFM spin state, driving a switch from the FM state, but as the electron–neutral distance increases, the external electric field felt by the Gd_2O_2 neutral goes to zero, and the AFM and FM states return to their unperturbed energies order, which in turn, slows the departing electron so that it reflects the unperturbed energy of the final state which would not have been observed without the switch.

Table 2 includes assignments based on the following: The narrowest features that increase in intensity with decreasing photon energy (decreasing electron momentum) are assigned to the AFM states that are not expected to be observed in a "sudden" detachment formulation. The intense narrow features observed with highest photon energy are assigned to the neutral states in which the total spin of electrons occupying outer valence orbitals is zero, which may result in a very small axial zero-field splitting parameter, and the broader transitions are assigned to neutral FM-coupled states with parallel spins between the outer-valence electrons.

DISCUSSION

There are two principle findings that arise from the results of this study. The first involves the strong electron-neutral interactions that change the relative energy ordering of FM and AFM states of Gd_2O_2, and the second involves the prevalence of PEVE interaction-driven transitions that fall outside of a one-electron description.

At first glance, assignment of the group of transitions to the low-lying neutral states accessed via direct detachment of electrons from the close-lying, non-bonding $\sigma_{6s,g}$ and $\sigma_{6s,u}$ (manifold **I**) is straightforward, given the relatively simple appearance of the spectrum obtained with 3.495 eV photon

energy and the agreement between the observed and predicted detachment energies. However, the emergence of and intensity changes exhibited by narrow features (X′, A, a), the broader grouping of close-lying transitions (B) with decreasing photon energy is compelling evidence that the detachment process is more complex. Broad vibrational progressions are inapposite with the diffuse and non-bonding nature of the $\sigma_{6s,g}$ and $\sigma_{6s,u}$ orbitals, and extended vibrational transitions are not predicted by the calculations. The more likely explanation is that certain electronic transitions are exhibiting a splay of M_s states, giving an axial zero-field coupling constant on the order of -15 cm^{-1} for certain, but not all, states. Our results suggest that neutral states in which the spins of the two outer-valence electrons are parallel have this larger coupling constant, while states with zero spin in the outer-valence orbitals have a smaller coupling constant.

The external electric field introduced by the photoelectron approaches zero as the electron-neutral distance increases with time, but on the fs timescale, it remains over 0.4 V·Å^{-1}, which is on the order of fields that can switch the relative energies of FM and AFM coupled states studied using scanning-tunneling electron microscopy tips.[48] As the photon energy is decreased, the time the ejected electron lies in a range that can induce the change in relative FM and AFM state energies increases, potentially switching an FM neutral remnant to an AFM neutral remnant, but if the state cannot switch back to FM as the field decays with electron-neutral distance, the final less stable neutral state's unperturbed energy will be encoded in the electron kinetic energy, and reflected as increased intensity of narrow transitions embedded among the transitions that can be characterized as direct detachment transitions.

The prevalence of transitions that cannot be characterized as strictly one-electron has been noted in previous studies on samarium suboxide clusters, with Sm_2O^- studied in the greatest detail.[19] In the "sudden" framework, manifold **I** in the $Gd_2O_2^-$ PE spectrum consists largely of transitions from the FM-coupled $^{16}B_{1u}$ anion to the five one-electron allowed (assuming spin is not a good quantum number) FM-coupled neutral states. Manifold **II** goes beyond simple spin change violations, in that no neutral states in

this energy range are accessible via changing the orbital occupancy by one electron. Instead, all states would be accessible by shakeup transitions due to PEVE interactions, which become more pronounced with decreasing photon energy and photoelectron momentum.

While not explicitly described as such, an intense group of excited state transitions in the PE spectrum of GdO^- was assigned to a shake-up transition as well.[32] These ca. 1 eV excitations appear to be general for systems with doubly occupied 6s-based MOs, underscoring the role of the polarizability of the remnant neutral by the photoelectron being conducive to two-electron excitation.

Because the electronic structure of $Gd_2O_2^-$ is fundamentally simpler than that of Sm_2O^-, the non-monotonic changes in the relative intensities of individual transitions with decreasing photon energy (i.e., e^-KE) was more readily observed. While analyzing correlations and anti-correlations between the intensities of the crush of transitions in manifold is beyond the scope of this paper, the oscillations in the peak intensities with photon energy that are clearly evident in the contour plot (Figures 5 and 6) suggest a need to expand our theoretical platform to account for interference between different one- and two-electron detachment pathways. Clearly, these small molecules challenge our current understanding of electron detachment and electron-neutral interactions (or PEVE interactions) and correlation of electrons in diffuse orbitals with close-lying core-like orbitals with high spin.

METHODS

Experimental Details. $Gd_2O_2^-$ was generated and spectroscopically probed in an apparatus that has been described in detail previously.[19,49,50] Approximately 7-8 mJ/pulse of the second harmonic output of a Nd:YAG laser (532 nm, 2.33 eV) operating at 30 Hz ablated the surface of a rotating compressed Gd powder (Alfa Aesar, 99.9%) target. A pulse of ultra-high purity He introduced from a pulsed molecular beam valve swept the resultant plasma through a 25 mm long, 3 mm diameter clustering channel. The gas mixture then expanded into vacuum and the anions were mass analyzed in a time-of-flight mass spectrometer. $Gd_2O_2^-$ was selectively photodetached by a fixed frequency laser in the ion-photon

interaction region, located 15 cm upstream of the ion detector. A small fraction (10^{-4}) of the photoelectrons travelled the length of a 1 m field-free drift tube orthogonal to the ion drift tube and collided with a second dual MCP detector assembly, the output of which was recorded to measure the photoelectron drift times, then converted to e^-KE, and subsequently e^-BE.

Spectra were calibrated by measuring the PE spectrum of O^- at all photon energies, and performing a linear fit on the electron drift times as a function of $(e^-KE - E_{corr})^{-1/2}$, where e^-KE is the expected electron kinetic energy of the highest e^-KE O^- detachment signal based on the photon energy, and E_{corr} is the laboratory to center-of-mass frame correction term; the slope is proportional to the drift tube length, and the intercept is t_0. The electron signal totals were binned, and the electron signal from 0.8 to 1.8 eV was normalized to 1 for each spectrum.

Spectra were measured with laser polarization both parallel ($\theta = 0° \pm 10°$) and perpendicular ($\theta = 90° \pm 10°$) to the direction of electron detection to gauge photoelectron angular distribution (PAD), and to discern overlapping transitions that are common in these under-coordinated metal-oxide clusters. All of the spectra presented were accumulated over 500,000 to 1,500,000 laser shots.

Computational Details. Calculations were carried out using the Gaussian suite of electronic structure programs.[39,40] Results described above employed the B3LYP/ANO-ECPplusPVTZ model chemistry. The ANO-ECPplusPVTZ incorporates the the Stuttgart relativistic small-core atomic natural orbital basis set and effective core potential and corresponding valence basis set for Gd and a Dunning-style correlation consistent basis set for O.[41,42] All converged Kohn-Sham determinants were characterized using stability calculations.[43,44] Spin contaminated determinants were treated using spin purification models.[515253] Electron detachments modeled by DFT calculations were characterized using the natual ionization orbital model.[54] Geometry optimizations were carried out using standard techniques and potential energy surface stationary points were characterized using analytic second-derivative calculations.[45] Reported energies include zero-point energy corrections.

We note that for molecules with exceptionally complex electronic structures, such as cases where energy gaps are on the order a few-tenths of an eV and where the true electronic structure may be multi-determinantal, DFT results must be considered with caution. As described in the supplementary information, such care was taken in this work. Preliminary analysis fully supports the model chemistry chosen here for the interpretive and simulated spectra included.

Data availability. The data supporting the findings of this study are available from the corresponding authors upon request.

Acknowledgements

We are grateful for invaluable communication with Prof. Michael Heaven and Dr. Leonid Kaledin, and support from the Indiana University College of Arts and Sciences. HPH is grateful for generous support from the National Science Foundation (CHE-1848580) and acknowledges computing time on the Multi-Environment Computer for Exploration and Discovery (MERCED) cluster which was supported by the National Science Foundation (Grant No. ACI-1429783).

Author contributions

C.C.J. conceived the experiments, J.L.M., A.J.M, and C.D.H. conducted the experiments, J.L.M. completed preliminary DFT calculations and liaised with the UC Merced group, H.P.H. conceived computational workflow and computational methods used, H.H. implemented computational methodologies and carried out DFT calculations and analysis, A.A.T. and H.C. implemented computational methods.

Additional Information

Supplementary information is available in the online version of the paper.

Competing Financial Interests

The authors declare no competing financial interests.

REFERENCES

(1) Antonov, V. N.; Bekenov, L. V.; Yaresko, A. N. Electronic Structure of Strongly Correlated Systems. *Adv. Cond. Matt. Phys*. **2011**, *2011*, 298928 1-107.

(2) Monroe, C.; Campbell, W. C.; Duan, L. -M.; Gong, Z. -X.; Gorshkov, A.V.; Hess, P.; Islam, R.; Kim, K.; Pagano, G.; Richerme, P.; Senko, C.; Yao, N. Y. Programmable Quantum Simulations of Spin Systems with Trapped Ions. Ion Traps for Tomorrow's Applications. *Proc. Int. School Phys. Enrico Fermi* **2015**, *189*, 169-187.

(3) Gould, C. A.; McClain, K. R.; Yu, J. M.; Groshens, T. J.; Furche, F.; Harvey, B. G.; Long, J. R. Synthesis and Magnetism of Neutral, Linear Metallocene Complexes of Terbium(II) and Dysprosium(II). *J. Am Chem. Soc.* **2019**, *141* 12967-12973.

(4) Tokmachev, A. M.; Averyanov, D. V.; Taldenkov, A. N.; Parfenov, O. E.; Karateev, I. A.; Sokolov, I. S.; Storchak V. G. Lanthanid f^7 Metalloxenes- a Class of Intrinsic 2D Ferromagnets. *Mat. Horiz*. **2019**, *6*, 1488-1496.

(5) Field, R.W. Diatomic Molecule Electronic Structure beyond Simple Molecular Constants. *Ber. Bunsenges. Phys. Chem.* **1982**, *86*, 771-779.

(6) Kaledin, L. A.; McCord, J. E.; Heaven, M. C. Laser Spectroscopy of CeO: Characterization and Assignment of States in the 0-3 eV Range. *J. Molec. Spectrosc* . **1993**, *158*, 40-61.

(7) Kaledin, L. A.; McCord, J. E.; Heaven, M.C. Rotation-Electronic Deperturbation Analysis of the 4*f* 6*s* Configurational States of CeO. *J. Molec. Spectrosc.* **1995**, *170*, 166-171.

(8) Carette, P. and Hocquet, A. Ligand Field Calculation of the Lower Electronic Energy levels of the Lanthanide Monoxides. *J. Molec. Spectrosc.* **1988**, *131*, 301-324.

(9) Kafader, J. O.; Topolski, J. E.; Colon, V. M.; Iyengar, S. S.; Jarrold, C. C. The Electron Shuffle: Cerium Influences Samarium 4*f* Orbital Occupancy in Heteronuclear Ce-Sm Oxide Clusters. *J. Chem. Phys.* **2017**, *146*, 194310.

(10) Topolski, J. E.; Kafader, J. O.; Colon, V. M.; Iyengar, S. S.; Hratchian, H. P.; Jarrold, C. C. Exotic Electronic Structures of $Sm_xCe_{3-x}O_y$ (x = 0-3; y = 2-4) Clusters, and the Effect of High Neutral Density of Low-Lying States on Photodetachment Transition Intensities. *J. Chem. Phys.* **2018**, *149*, 054305.

(11) Mason, J. L.; Harb, H.; Topolski, J. E.; Hratchian, H. P.; Jarrold, C. C. Exceptionally Complex Electronic Structures of Lanthanide Oxides and Small Molecules. *Acc. Chem. Res.* **2019**, *52*, 3265-3273.

(12) Wigner, E. P. On the Behavior of Cross Sections Near Thresholds. *Phys. Rev.* **1948**, *73*, 1002-1009.

(13) Parkes, M. A.; Bennett, A.;H.H. Fielding, H. H. *J. Mol. Phys.* **2019**, *117*, 3027-3035.

(14) Bull, J. N.; Anstoter, C. S.; Verlet, J. R. R. Ultrafast Valence to Non-Valence Excited State Dynamics in a Common Anionic Chromophore. *Nat. Commun*. 2019, *10*, 5820 1-9.

(15) Mensa-Banu, G.; Wilson, M. R.; D.J. Tozer, D. J.; Verlet, J. R. R. Photoelectron Spectroscopy of Para-benzoquinone Cluster Anions. *J. Chem. Phys.* **2019**, *151*, 204302.

(16) Lyle, J.; Jagau, T. -C.; R. Mabbs, R. Spectroscopy of Temporary Anion States: Renner-Teller Coupling and Electronic Autodetachment in Copper Difluoride Anion. *Faraday Disc.* **2019**, *217*, 533-546.

(17) Zhu, G. -Z. and Wang, L. -S. High-Resolution Photoelectron Imaging and Resonant Photoelectron Spectroscopy via Noncovalently Bound Excited States of Cryogenically Cooled Anions. *Chem. Sci.* **2019**, *10*, 9409-9423.

(18) Thurston, G. K.; Sagan, C. R.; Garand, E. Vibrationally Resolved Photoelectron Spectroscopy of Oligothiophene Radical Anions. *J. Chem. Phys*. **2019**, *151*, 165401.

(19) Mason, J. L.; Topolski, J. E.; Ewigleben, J. C.; Iyengar, S. S.; Jarrold, C. C. Photoelectrons are not Always Quite Free. *J. Phys. Chem. Lett.* **2019**, *10*, 144-149.

(20) La Cava, F.; Mingo, A. F.; Miragoli, L.; Terreno, E.; Cappelletti, E.; Lattuada, L.; Poggi, Luisa; Serra, S. C. Synthesis, Characterization, and Biodistribution of a Dinuclear Gadolinium Complex with Improved Properties as a Blood Pool MRI Agent. *ChemMedChem*. **2018**, *13*, 824-834.

(21) Kafader, J. O.; Topolski, J. E.; Jarrold, C. C. Molecular and Electronic Structures of Cerium and Cerium Suboxide Clusters. *J. Chem. Phys.* **2016**, *145*, 154306 1-17.

(22) Topolski, J. E.; Kafader, J. O.; Ray, M.; Jarrold, C. C. Elucidating Cerium + H_2O Reactivity Through Electronic Structure: A Combined PES and DFT Study. *J. Mol. Spec.* **2017**, *336* 1-11.

(23) Ray, M.; Felton, J. A.; Kafader, J. O.; Topolski, J. E.; Jarrold, C. C. Photoelectron spectra of CeO^- and $Ce(OH)_2^-$. *J. Chem. Phys.* **2015**, *142*, 054305 1-8.

(24) Kafader, J. O.; Ray, M.; Jarrold, C. C. Photoelectron Spectrum of PrO^-. *J. Chem. Phys.* **2015**, *143*, 064305 1-6.

(25) Kafader, J. O.; Ray, M.; Jarrold, C. C. Low-lying Electronic Sturtcure of EuH, EuOH, and EuO Neutrals and Anions Determined by Anion Photoelectron Spectroscopy and DFT Calculations. *J. Chem. Phys.* **2015**, *142*, 034305.

(26) Topolski, J. E.; Kafader, J. O.; Jarrold, C. C. Ce in the +4 Oxidation State: Anion Photoelectron Spectroscopy and Photodissociation of Small $Ce_xO_yH_z^-$ Molecules. *J. Chem. Phys.* **2017**, *147*, 104303 1-10.

(27) Ray, M.; Kafader, J. O.; Topolski, J. E.; Jarrold, C. C. Mixed Cerium-Platinum Oxides: Electronic Structure of $[CeO]Pt_n$ (n = 1, 2) and $[CeO_2]Pt$ complex anions and neutrals. *J. Chem. Phys.* **2016**, *145*, 044317 1-10.

(28) Mason, J. L.; Harb, H.; Topolski, J. E.; Hratchian, H. P.; Jarrold, C. C. A Tale of Two Stabilities: How One Boron Atom Affects a Switch in Bonding Motifs in $CeO_2B_x^-$ (x = 2, 3) Complexes. *J. Phys. Chem. A* **2018**, *122*, 9879-9885.

(29) Mason, J. L.; Harb, H.; Huizenga, C. D.; Ewigleben, J. C.; Topolski, J. E.; Hratchian, H. P.; Jarrold, C. C. Electronic and Molecular Structures of the CeB_6 Monomer. *J. Phys. Chem. A* **2019**, *123*, 2040-2048.

(30) Messiah, A. *Quantum Mechanics*; John Wiley & Sons, Inc.: New York, U.S.A.; 1966.

(31) Kaledin, L. A.; Erickson, M. G.; Heaven, M. C. Laser Spectroscopy of GdO: Ligand Field Assignments of $4f^7(^8S)6p \leftarrow 4f^7(^8S)6s$ Transitions. *J. Molec. Spectrosc.* **1994**, *165*, 323-333.

(32) Klingeler, E.; Pontius, N. Lüttgens, G.; Bexhthold, P. S.; Neeb, M.; Eberhardt, W. Photoelectron Spectrsocopy of GdO^-. *Phys. Rev. A.* **2002**, *65*, 032502.

(33) Roy, L.E.; Hughbanks, T. Magnetic Coupling in Dinuclear Gd Complexes. *J. Am. Chem. Soc*. **2006**, *128*, 568-575.

(34) Rinehart, J. D.; Fang, M.; Evans, W. J.; Long, J. R. Strong Exchange and Magnetic Blocking in N_2^{3-} Radical-Bridged Lanthanide Complexes. *Nat. Chem*. **2011**, *3*, 538–542.

(35) Meihaus, K. R.; Corbey, J. F.; Fang, M.; Ziller, J. W.; Long, J. R.; Evans, W. J. Influence of an Inner-Sphere K+ Ion on the Magnetic Behavior of N_2^{3-} Radical-Bridged Dilanthanide Complexes Isolated Using an External Magnetic Field. *Inorg. Chem*. **2014**, *53*, 3099–3107.

(36) Weichman, M.L.; Vlaisavljevich, B.; DeVine, J.A.; Shuman, N.S.; Ard, S.G.; Shiozaki, T.; Neumark, D.M.; Viggiano, A.A. Electronic Structure of SmO and SmO^- via Slow Photoelectron Velocity-Map Imaging Spectroscopy and Spin-Orbit CASPT2 Calculations. J. Chem. Phys. **2017**, *147*, 234311.

(37) Yoder, B.L.; Maze, J.T.; Raghavachari, K.; Jarrold, C.C. Structures of $Mo_2O_y^-$ and Mo_2O_y (y = 2, 3, and 4) studied by anion photoelectron spectroscopy and density functional theory calculations, *J. Chem. Phys*. **2005**, *122*, 094313.

(38) Van Zee, R.J.; Ferante, R.F.; Zerigue, K.J.; Weltner, Jr., W. The Ground State and Zero-field Splitting of the GdO Molecule, *J. Chem. Phys*. **1982**, *75*, 5297-5299.

(39) Costes, J.P.; Dahan, F.; Nicodeme, F. A Trinuclear Gadolinium Complex: Structure and Magnetic Properties. *Inorg. Chem*. **2001**, *40*, 5285–5287.

(40) Yuan, D.-F.; Liu, Y.; Qian, C.-H.;Kocheril, G.S.; Zhang, Y.-R.; Rubenstein, B.M.; Wang, L.-S. Polarization of Valence Orbitals by the Intramolecular Electric Field from a Diffuse Dipole-Bound Electron, *J. Phys. Chem. Lett.* **2020**, *11*, 7914.

(41) Langer, B.; Viefhaus, J.; Hemmers, O.; Manzel, A.; Wehlitz, M. R.; Becker, U. High-resolution Photoelectron Spectrometry Study of Conjugate Shakeup Processes in the Li 1s Threshold Region. *Phys. Rev. A.* **1991**, *43*, 1652.

(42) Randall, K. J.; Kilcoyne, A. L. D.; Koppe, H. M.; Feldhaus, J.; Bradshaw, A. M.; Rubensson J-. E.; Eberhardt, W.; Xu, Z.; Johnson, P. D.; Ma, Y. Photon Energy Dependence of the High Resolution C 1s Photoelectron Spectrum of CO in the Threshold Region. *Phys. Rev. Lett.* **1993**, *71*, 1156.

(43) Fechner, M.; Zahn, P.; Ostanin, S.; Bibes, M.; Mertig, I. Switching Magnetization by 180° with an Electric Field. *Phys. Rev. Lett.* **2012**, *108*, 197206.

(44) Yun, K-. H.; Lee, M.; Chung, Y-. C. Electric Field as a Novel Switch for Magnetization of Fe/graphene System. *J. Magn. Magn. Mater.* **2014**, *362*, 93-96.

(45) Barnes, S. E.; Ieda, J.; Maekawa, S. Rashba Spin-Orbit Anisotropy and the Electric Field Control of Magnetism. *Sci. Rep.* **2014**, *4*, 4105.

(46) Zhou, Z.; Trassin, M.; Gao, Y.; Gao, Y.; Qiu. D.; Ashraf, K.; Nan, T.; Yang, X.; Bowden, S. R.; Pierce, T. D.; et al. Probing Electric Field Control of Magnetism Using Ferromagnetic Resonances. *Nat. Commun.* **2015**, *6*, 6082.

(47) Wang, W-. G.; Li, M.; Hageman, S.; Chien, C. L. Electric-Field-Assissted Switching in Magnetic Tunnel Junctions. *Nat. Mater.* **2012**, *11*, 64-68.

(48) Negulyaev, N. N.; Stepanyuk, V. S.; Hergert, W.; Kirschner, J. Electric Field as a Switching Tool for Magnetic States in Atomic-Scale Nanostructures. *Phys. Rev. Lett.* **2011**, *106*, 037202.

(49) Moravec, V. D.; Jarrold, C. C. Study of the Low-Lying States of NiO^- and NiO Using Anion Photoelectron Spectroscopy. *J. Chem. Phys.* **1998**, *108*, 1804-1810.

(50) Waller, S. E.; Mann, J. E.; Jarrold, C. C. Asymmetric Partitioning of Metals among Cluster Anions and Cations Generated via Laser Ablation of Mixed Aluminum/Group 6 Transition Metal Targets. *J. Chem Phys. A.* **2013**, *117*, 1765-1772.

[51] Hratchian, H. P. An Efficient Analytic Gradient Theory for Approximate Spin Projection Methods. *J. Chem. Phys.* **2013**, *138*, 101101.

[52] Thompson, L. M.; Hratchian, H. P. Second Derivatives for Approximate Spin Projection Methods. *J. Chem. Phys.* **2015**, *142*, 054106.

[53] Thompson, L. M.; Hratchian, H. P. On Approximate Projection Models. *Mol. Phys.* **2019**, *310*, 1–9.

[54] Thompson, L. M.; Harb, H.; Hratchian, H. P. Natural Ionization Orbitals for Interpreting Electron Detachment Processes. *J. Chem. Phys.* **2016**, *144*, 204117.

Table 1. Summary of zero-point corrected relative energies of GdO/GdO^- and Gd_2O_2/$Gd_2O_2^-$ electronic states calculated at the B3LYP level of theory. The experimental energies and ligand field theory (LFT) calculations are provided for comparison.

	Electronic Structure	DFT Relative Energy (eV)	Exp. Relative Energy (eV)	LFT
GdO	$^9\Sigma$ ($4f^7\ \sigma_{6p}^{\alpha}$)	2.54	2.62[a]	2.61[a]
	$^9\Pi$ ($4f^7\ \pi_{6p}^{\alpha}$)	1.90	2.34[a]	2.18[a]
	$^9\Delta$ ($4f^7\ \delta_{5d}^{\alpha}$)	1.39	---	1.44[b]
	$a^7\Sigma$ ($4f^7\ \sigma_{6s}^{\beta}$)	0.27	0.23[a]	0.25[b]
	$X^9\Sigma$ ($4f^7\ \sigma_{6s}^{\alpha}$)	0	0	0
GdO^-	$^8\Sigma$ ($4f^7\ \sigma_{6s}^2$)	e^-BE = 1.05	1.19[c]	

		DFT Optimized Energy (eV)	Gd-Gd Internuclear Distance (Å)	Optimized Gd–O–Gd Angle (°)
Gd_2O_2	$^{17}B_{2g}(4f_a^{7,\alpha}4f_b^{7,\alpha}\sigma_{6s}^{1,\alpha}\pi_{5d}^{1,\alpha})$	2.42	3.13	100
	$^1A'\ \ (4f_a^{7,\alpha}4f_b^{7,\beta}\sigma_{6s}^{1,\beta}\sigma_{6s}^{*1,\alpha})$	1.72	3.12	100
	$^{15}B_{1u}(4f_a^{7,\alpha}4f_b^{7,\alpha}\sigma_{6s}^{1,\beta}\sigma_{6s}^{*1,\alpha})$	1.71	3.12	100
	$^{13}B_{1u}(4f_a^{7,\alpha}4f_b^{7,\alpha}\sigma_{6s}^{1,\beta}\sigma_{6s}^{*1,\beta})$	1.45	3.13	100
	$^3A'\ \ (4f_a^{7,\alpha}4f_b^{7,\beta}\sigma_{6s}^{1,\alpha}\sigma_{6s}^{*1,\alpha})$	1.18	3.13	99
	$^{15}A_g(4f_a^{7,\alpha}4f_b^{7,\alpha}\sigma_{6s}^2)$	1.08	3.08	99
	$^{17}B_{1u}(4f_a^{7,\alpha}4f_b^{7,\alpha}\sigma_{6s}^{1,\alpha}\sigma_{6s}^{*1,\alpha})$	0.93	3.14	99
	$^1A'\ \ (4f_a^{7,\alpha}4f_b^{7,\beta}\sigma_{6s}^2)$	0.78	3.13	99
$Gd_2O_2^-$	$^{14}B_{1u}(4f_a^{7,\alpha}4f_b^{7,\alpha}\sigma_{6s}^2\sigma_{6s}^{*1,\beta})$	0.18	3.12	99
	$^2A'\ \ (4f_a^{7,\alpha}4f_b^{7,\beta}\sigma_{6s}^2\sigma_{6s}^{*1,\alpha})$	0.07	3.13	99
	$^{16}B_{1u}(4f_a^{7,\alpha}4f_b^{7,\alpha}a_{g,6s}^2b_{1u,6s}^{\alpha})$	0.00	3.12	99

[a] Ref [31]

[b] Ref [8]

[c] Ref [32]

Table 2. Summary of peak positions and tentative assignments. Red text indicates states that are not allowed *via* one-electron transitions.

Peak	Position (e^-BE/eV)	Final Neutral State	
		e^- configuration	Electronic term
Manifold **I**			
X	ADE = 0.97(3) VDE = 1.052	$4f_a^{7\alpha}4f_b^{7\alpha}\,\sigma_{6s.g}^{\alpha}\sigma_{6s,u}^{\alpha}$	$^{17}B_{1u}$
X′	1.060(5)	$4f_a^{7\alpha}4f_b^{7\beta}\sigma_{6s,g}^{2}$	$^{1}A_g$
A	1.142(5)	$4f_a^{7\alpha}4f_b^{7\alpha}\sigma_{6s,g}^{2}$	$^{15}A_g$
a	1.219(5)	$4f_a^{7\alpha}4f_b^{7\beta}\,\sigma_{6s.g}^{\alpha}\sigma_{6s,u}^{\alpha}$	$^{3}B_{1u}$
b	1.24-1.30	$4f_a^{7\alpha}4f_b^{7\alpha}\,\sigma_{6s.g}^{\beta}\sigma_{6s,u}^{\beta}$	$^{13}B_{1u}$
B	1.25-1.36	?	?
c	1.390(10)	$4f_a^{7\alpha}4f_b^{7\alpha}\,\sigma_{6s.g}^{\alpha}\sigma_{6s,u}^{\beta}$	$^{15}B_{1u}$
		$4f_a^{7\alpha}4f_b^{7\alpha}\,\sigma_{6s.g}^{\beta}\sigma_{6s,u}^{\alpha}$	$^{15}B_{1u}$
		$4f_a^{7\alpha}4f_b^{7\beta}\,\sigma_{6s.g}^{\alpha}\sigma_{6s,u}^{\beta}$	$^{1}B_{1u}$
d	1.49(3)	?	?
Manifold **II**			
e	2.15		
f	2.27		
g	2.42		